

Modeling of a Nickel-based Fluidized Bed Membrane Reactor for Steam Methane Reforming Process

¹Mustafa Kamal Pasha, ¹Iftikhar Ahmad*, ¹Jawad Mustafa, ²Manabu Kano

¹Dept. of Chemical Engineering, School of Chemical and Materials Engineering (SCME), National University of Sciences and Technology (NUST), Islamabad 44000, H-12.

²Dept. of Systems Science, Kyoto University, Yoshida-Honmachi, Sakyo-ku, Kyoto, 606-8501, Japan. Iftikhar.salarzai@scme.nust.edu.pk*

(Received on 21st November 2017, accepted in revised form 26th September 2018)

Summary: Hydrogen being a green fuel is rapidly gaining importance in the energy sector. Steam methane reforming is one of the most industrially important chemical reaction and a key step in the production of high purity hydrogen. Due to inherent deficiencies of conventional reforming reactors, a new concept based on fluidized bed membrane reactor is getting the focus of researchers. In this work, a nickel-based fluidized bed membrane reactor model is developed in the Aspen PLUS® process simulator. A user-defined membrane module is embedded in the Aspen PLUS® through its interface with Microsoft® Excel. Then, a series combination of Gibbs reactors and membrane modules are used to develop a nickel-based fluidized bed membrane reactor. The model developed for nickel-based fluidized bed membrane reactor is compared with palladium-based membrane reactor in terms of methane conversion and hydrogen yield for a given panel of major operating parameters. The simulation results indicated that the model can accurately predict the behavior of a membrane reactor under different operating conditions. In addition, the model can be used to estimate the effective membrane area required for a given rate of hydrogen production.

Keywords: Membrane reactor, Steam methane reforming, Aspen PLUS®, Excel®, Nickel membrane, Hydrogen, Modeling, Simulation.

Introduction

Methane steam reforming is a predominant method for the production of synthesis gas, which has potential use in ammonia and methanol production, Fischer-Tropsch synthesis and other important petrochemical and petroleum refining process [1]. Conventionally steam methane reforming is carried out in fixed bed reformer. These reformers typically consist of a number of tubes packed with catalyst. The conventional reformers have many disadvantages like poor heat transfer rate, coke formation on the catalyst surface, thermodynamic equilibrium limitations, large temperature gradient etc. [2]. To overcome these limitations, a new concept of fluidized bed membrane reactor is introduced in the recent years that showed convenient results at bench and pilot scale.

The fluidized bed membrane reactor (FBMR) is multi-functional in their operation. It can produce highly pure hydrogen with high methane conversion in a single step. Whereas, the conventional industrial reforming process needs many stages to gain the desired conversion for methane and carbon monoxide and needs further separation steps to separate hydrogen from the reactor outlet. Moreover, the hydrogen separation through membrane enhances methane conversion and hydrogen yield by shifting the reaction equilibrium

towards the product [3-5]. Furthermore, it has a uniform temperature in the catalyst bed and good heat transfer capability as compared to conventional fixed bed reactors [6]. Despite these advantages, very few attempts have been reported in the literature on the industrial commercialization of membrane reactor because of complexity in the scale-up, technological difficulties, and economics. Moreover, a number of experiments are needed to study the effects of different operating conditions on the performance of membrane reactors but, there are some difficulties in carrying out these experiments such as the controllability of operating variables, complex operational concerns, proper maintaining of highly expensive membrane tubes, and tedious experiments involved. When the reformer is modeled, these effects could be investigated while saving time without a further need to generate highly expensive data [20].

Various models have been proposed to model FBMR. Adris (1997) proposed a two-phase bubbling bed model for steam methane reforming with hydrogen separation through the membrane. Later on, this model was extended to model auto-thermal steam reforming with oxygen addition by Dogan (2003) and Roy (1998). Grace (2001) modeled the FBMR with oxygen addition based on

*To whom all correspondence should be addressed.

thermodynamic equilibrium [2, 7-9]. The model was helpful in investigating the effect of different process parameters on reactor performance. Chen (2004) developed a model for a circulating FBMR that was based on a steady state one-dimensional PFR model [10]. All these models were solved by MATLAB®, FORTRAN or other computer programs, which are not easily accessible to design engineers in industry. Various process simulators, such as Aspen PLUS® and Aspen HYSYS®, are employed widely for industrial process simulations which include built-in standard and ideal unit operation models. Moreover, these simulators also provide a tool to integrate a user defined module in their simulation environment. Server-Amini (2007) modeled the membrane reactor for steam methane reforming process using the environment of Aspen PLUS® [20]. The model consists of the combination of CSTR and PFR with mass transfer calculation blocks. The mass transfer blocks were used to calculate the hydrogen permeation through a membrane inside the reactor. In another approach, the process was simulated by using the sequential modular simulation method [21] in which Gibbs reactor integrated with FORTRAN sub-routine was used to develop palladium-based FBMR model. The developed model had successfully investigated the effect of different operating parameters on the reactor performance. However, the integrated FORTRAN sub-routine is limited to a specific membrane case and cannot be used to test the effect of different hydrogen perm-selective membranes on the reactor performance. Moreover, FORTRAN language is not widely used now as the language is very old and not user-friendly. The present work aims to fill this gap by interfacing Excel with Aspen PLUS®. Excel provides an easier way to simulate the FBMR process in a more user-friendly environment as compared to FORTRAN sub-routine. In addition, Excel® is flexible enough to extend the capability of the model to test the effect of other types of membranes on the reactor performance.

In this work, a nickel-based fluidized bed membrane reactor model is developed using Aspen PLUS®-Excel® interfacing. Experimental data is not available for nickel-based fluidized bed membrane reactor. However, for palladium based FBMR both the simulated and experimental data are available in the literature. Therefore, the nickel-based FBMR model is simulated and validated by comparison with the palladium-based FBMR [21]. The performance of the nickel-based and the palladium-based FBMR are analyzed by investigating the impact of major operating parameters (reactor pressure, temperature, permeate side hydrogen partial pressure and steam feed rate) on methane conversion and hydrogen yield.

Then, the nickel and the palladium membrane area required for a fixed methane conversion and hydrogen yield at a fixed operating temperature are calculated for both reactors.

In this study, section 2 describes the process followed by nickel-based fluidized bed membrane reactor model development in section 3. Section 4 establishes the results and discussion while section 5 concludes the work.

Process Description

Fluidized Bed Membrane Reactor

Fluidized bed membrane reactor is a combination of chemical reactor and a membrane. A schematic diagram of a typical fluidized bed membrane reactor is shown in Fig 1. Pre-heated steam and methane are pre-mixed and then fed to the reactor where the following principal reforming reactions take place.

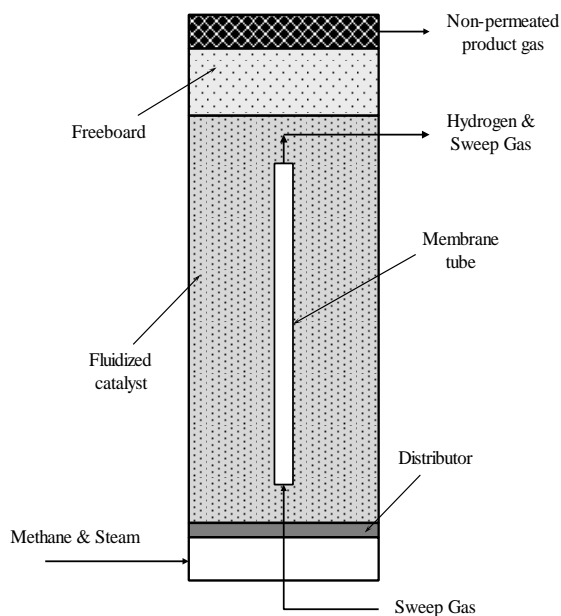


Fig. 1: Schematic diagram of a typical fluidized bed membrane reactor.

All of the above reactions are endothermic except reaction 2 (water-gas shift) which is exothermic. The reactions are carried out at high temperature (usually 450-850 °C) and high pressure (usually 1-3 MPa). Inside the bed, a number of

membrane tubes are installed that are selectively permeable to hydrogen. The catalyst bed is fluidized among the membrane tubes and steam reforming of methane takes place. As the synthesis gas is produced, hydrogen from the synthesis gas permeates through the membrane tubes. The permeated hydrogen is then carried away by a sweep gas (usually steam or nitrogen) to reduce hydrogen partial pressure on the permeate side.

Metallic Membranes

Among different types of membranes, dense metallic membranes are conventionally used in the membrane reactor area to separate hydrogen from gas mixtures. Hydrogen has high solubility and permeability in metallic membranes. Moreover, metallic membranes are stable enough at high operating temperatures and have a good mechanical stability. The most dominant materials for preparing this kind of membranes include palladium and its alloys, nickel, titanium, and vanadium [13].

The mechanism of hydrogen permeation through metallic membranes is based on the solution-diffusion model [11]. The steps that are involved in hydrogen transport from high to low-pressure region illustrated in Fig. 2 are the following: (1) diffusion of hydrogen molecules from bulk of the gas to the membrane surface, (2) dissociation of hydrogen molecule to hydrogen atoms and adsorption on membrane surface, (3) dissolution of hydrogen atoms into the bulk metal, (4) diffusion through the bulk metal to the permeate side, (5) association of hydrogen atoms on the membrane surface at the permeate side, (6) desorption of hydrogen molecules from the surface to bulk of the gas, and (7) diffusion to bulk of the gas from the membrane surface [3, 11].

Nickel-based Fluidized Bed Membrane Reactor Model Development

In this section, preliminary assumptions for model development, incorporation of membrane module within Aspen PLUS[®], sequential modular simulation of FBMR and determination of the number of sub-separators are discussed. The pre-exponential factor and activation energy are the main parameters that determine hydrogen permeability in metallic membranes and defines the type of membrane; the pre-exponential factor and activation energy for nickel membrane are $1.44 \times 10^{-6} \text{ mol m}^{-1} \text{ s}^{-1} \text{ Pa}^{-0.5}$ and $-51070 \text{ J mol}^{-1}$, respectively [14]. The nickel-based membrane module is incorporated in Aspen PLUS[®] by the method discussed earlier and the sequential modular method is employed to

simulate nickel-based fluidized bed membrane reactor. The developed model is simulated under different operating conditions and the results are compared with palladium-based FBMR for hydrogen production and methane conversion.

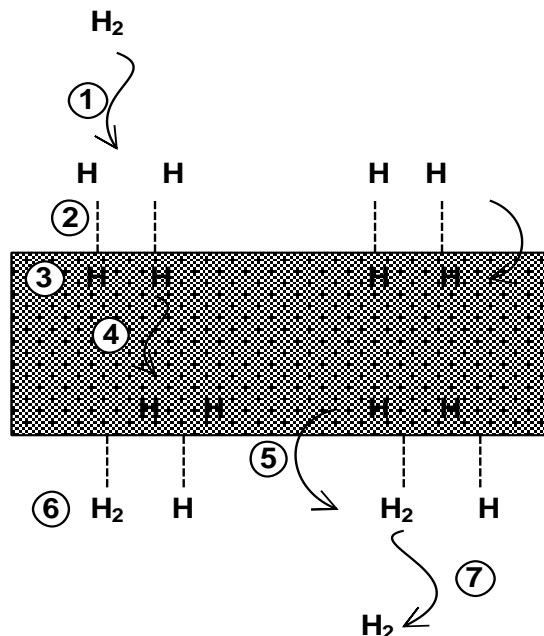


Fig. 2: Hydrogen permeation through metallic membranes [11].

Preliminary Assumptions

In the model development of membrane reactor within Aspen PLUS[®], several assumptions were made to simplify the methane steam reforming and hydrogen permeation process in the FBMR. The area under the dashed line in Fig. 3 is considered for the model development that assumes:

- 1) The flow of reaction gases is assumed plug flow, i.e. the composition of reaction gases varies only in the x-direction with negligible radial diffusion.
- 2) Temperature remains constant throughout the reactor.
- 3) There is no pressure gradient in the bed as well as in the membrane
- 4) All the reactions approach thermodynamic equilibrium locally i.e. Gibbs free energy is assumed to reach a minimum locally.
- 5) Hydrogen permeation through the membrane is ruled by Sieverts' law (Sieverts, 1935).

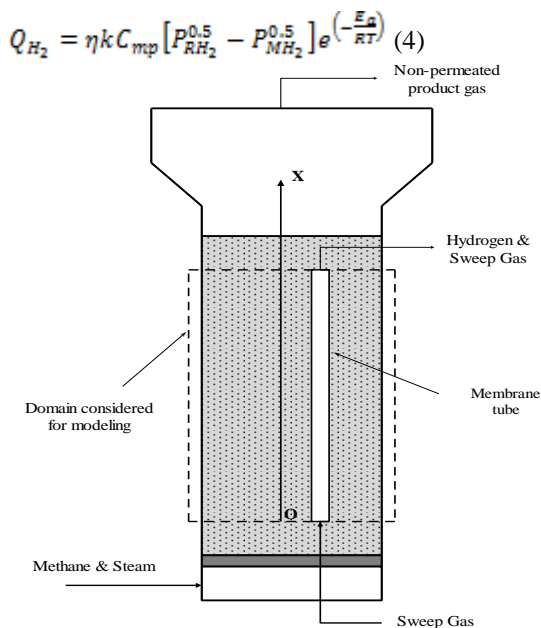


Fig. 3: Schematic diagram for modeling fluidized bed membrane reactor.

The membrane performance is negatively influenced by the co-existence of CO, H₂O, CO₂ or CH₄. The performance is also affected by non-uniformity in membrane fabrication and blockage of the membrane surface by catalyst dust. The membrane permeation effectiveness factor (η) account for all these negative influences on permeation rate and determined experimentally [15].

Simulation with Aspen PLUS®

Aspen PLUS® does not contain a built-in unit operation module for FBMR. To simulate the process within Aspen PLUS®, FBMR is sub-divided into methane sub-reformer and membrane sub-separator. The synthesis gas production process is carried out in methane sub-reformer while hydrogen permeation through membrane tubes is carried out in membrane sub-separator. Gibbs reactor module of Aspen PLUS® is employed as a methane sub-reformer. Membrane sub-separator is a user-defined membrane module based on Sieverts' law (Eq. 4), that is incorporated in Aspen PLUS® by Aspen PLUS®-Excel® interfacing. The following two sub-sections describe the membrane integration within Aspen PLUS® and the combination of Gibbs reactor with membrane module to simulate the overall FBMR process.

Incorporation of Membrane Module within Aspen PLUS®

Aspen PLUS® provides several interfaces for including custom models in Aspen PLUS® simulations. In the model library of Aspen PLUS®, there is a section

called user models which contain three different user models: User Model, User Model 2, and User Model 3. All of these user models use FORTRAN as a programming language. However, User Model 2 can also be linked with Microsoft Excel® to include different user-defined unit operations models within Aspen PLUS®.

To simulate hydrogen permeation process through membrane tube, User Model 2 unit operation block with an Excel® spreadsheet was used to perform the calculations. All the model equations, parameters, and variables were defined in the Excel® file. Aspen PLUS® supplies properties of the feed stream of the user model and some additional parameters (η , k , C_{mp} , E , R , T , P_{RH_2} and P_{MH_2}) to the Excel® spreadsheet. The additional parameters are shown in Table-1. The Excel® organizes this information and calculates product stream properties with hydrogen production rate (Q_{H_2}) based on Sieverts' law. This information is then returned to Aspen PLUS® interface and results are displayed. This two-way communication between Aspen PLUS® and Excel® is shown in Fig 4.

Table-1: Membrane design parameters used in simulation [11, 12].

Parameter	Value	Unit
Number of membrane tubes (N)	12	--
Tube thickness	0.2	mm
Total membrane surface area (A_m)	0.96	m ²
Membrane effectiveness factor (η)	0.39	--
Membrane permeation capacity (C_{mp}) (area/thickness)	0.4	km
Ideal gas constant (R)	8.3145	J/mol.K
Permeate side hydrogen partial pressure (P_{MH_2})	42000	Pa
Pre-exponential factor (k) (nickel membrane)	1.44×10^{-6}	mol/m.sec.Pa ^{0.5}
Pre-exponential factor (palladium membrane)	1.084×10^{-7}	mol/m.sec.Pa ^{0.5}
Activation energy (E_a) (nickel membrane)	-51070	J mol ⁻¹
Activation energy (E_a) (palladium membrane)	-9180	J mol ⁻¹

Sequential Modular Simulation of FBMR

To model and simulate FBMR within Aspen PLUS®, the reactor is sub-divided into a number of successive steam methane sub-reformers and membrane sub-separators as shown in Fig 5. To simulate synthesis gas production process in steam methane sub-reformer, Gibbs reactor was employed. Gibbs reactor predicts the equilibrium composition of the products by minimizing the total Gibbs free energy of the system. Reaction kinetics is not needed in Gibbs reactor model. However, the species present in product gas must be specified. The product gas species that are considered to form the reactor off-gas are CO₂, CO, H₂, CH₄, and H₂O. The hydrogen permeation process in the membrane sub-separator was simulated by integrating membrane module within Aspen PLUS® through Aspen PLUS®-Excel® interfacing as described in the previous section.

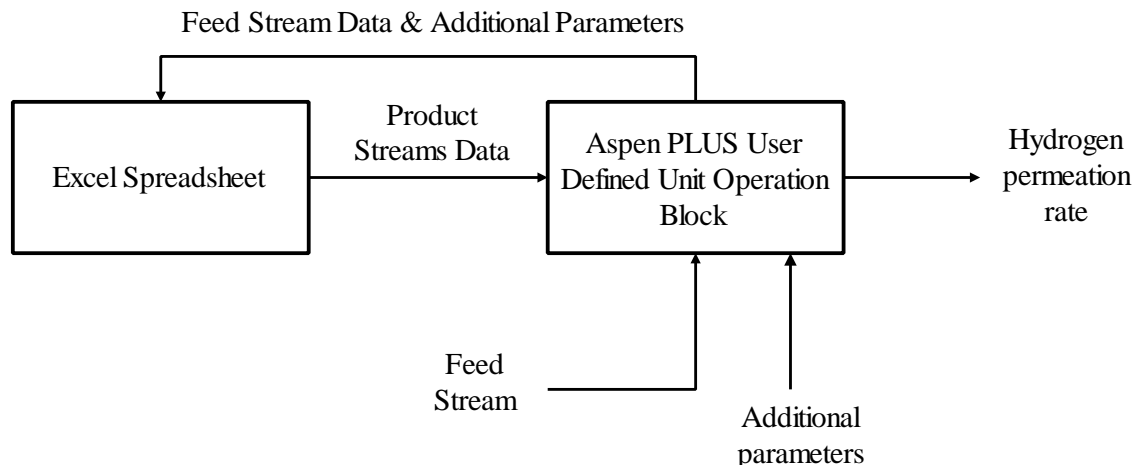


Fig. 4: Two-way communication between Aspen PLUS® and Microsoft Excel®.

The overall FBMR process illustrated in Fig 5 consists of $(n+1)$ sub-reformers and n sub-separators. Steam and methane that constitute the feed to the FBMR are fed to the first sub-reformer where the reaction takes place. The reactor off-gases are then fed to the first sub-separator where hydrogen is permeated through the membrane. Each membrane sub-separator which is employed for hydrogen permeation has permeation capacity of $C_{mp/n}$. The non-permeated gases are then fed to the 2nd sub-reformer. The permeated hydrogen from the 1st sub-separator accumulates in the 2nd sub-separator. In general, the reactor off-gases from i^{th} sub-reformer are introduced to the i^{th} sub-separator and the non-permeated gases from i^{th} sub-separator are introduced to the $(i^{\text{th}} + 1)$ sub-reformer. The reactor off-gases from $(i^{\text{th}} + 1)$ sub-reformer are then fed to the $(i^{\text{th}} + 1)$ sub-separator that also accumulates permeated hydrogen from i^{th} sub-separator. The same process is carried out for $(n+1)$ sub-reformers and n sub-separators.

Determination of Number of Sub-separators

The number of sub-separators in sequential modular approach method plays a critical role and it should be selected such that the method closely represents a real FBMR process. At $n = 0$, there is no sub-separator and the model represents only a fluidized bed Gibbs reactor. At $n = 1$, the model represents two sub-reformers and one sub-separator with total membrane permeation capacity of C_{mp} . For the case $n = 2$, the model has three sub-reformers and two sub-separators, where each sub-separator has same membrane permeation capacity of $C_{mp/n}$ ($n = 2$). With increase in number of sub-separators, the total membrane permeation capacity is equally divided among the sub-separators. The influence of

number of separator on hydrogen production rate for a typical case is shown in Fig 6. It can be seen that the change in the hydrogen production rate is negligible after $n > 50$ for all membrane permeation capacities. Therefore, the optimum number of sub-separators is taken 50 for this model

Model Validation with Palladium-based FBMR

For nickel-based FBMR experimental data is not available in the literature. Therefore, the modeling framework is first validated for palladium based FBMR whose experimental data is available in the literature, [12]. Adris (1994) carried out the steam methane reforming reaction between 720 to 930 K in a pilot plant palladium-based fluidized bed membrane reactor with methane and steam feed rate of 74.2 mol h^{-1} and $178.08 \text{ mol h}^{-1}$, respectively [12]. The reactor has a length of 1.143 m and a body diameter of 97 mm. Inside the reactor; twelve thin walled palladium membrane tubes were installed that are selectively permeable to hydrogen. 99.95 % pure palladium was used for tube fabrication. Each tube has 0.2-0.28 mm wall thickness and 14.7 mm outside diameter with a total membrane permeation capacity of 0.4 km. Table-2 compares the model predictions with the experimental data in terms of methane conversion, hydrogen production rate, and product gas composition. Methane conversion and hydrogen yield are calculated by the following formulae:

$$X_{CH_4} = \frac{F_{CH_4,initial} - F_{CH_4,final}}{F_{CH_4,initial}} \quad (5)$$

$$H_{2,yield} = \frac{Q_{H_2} \text{ (molar)}}{F_{CH_4} \text{ (molar)}} \quad (6)$$

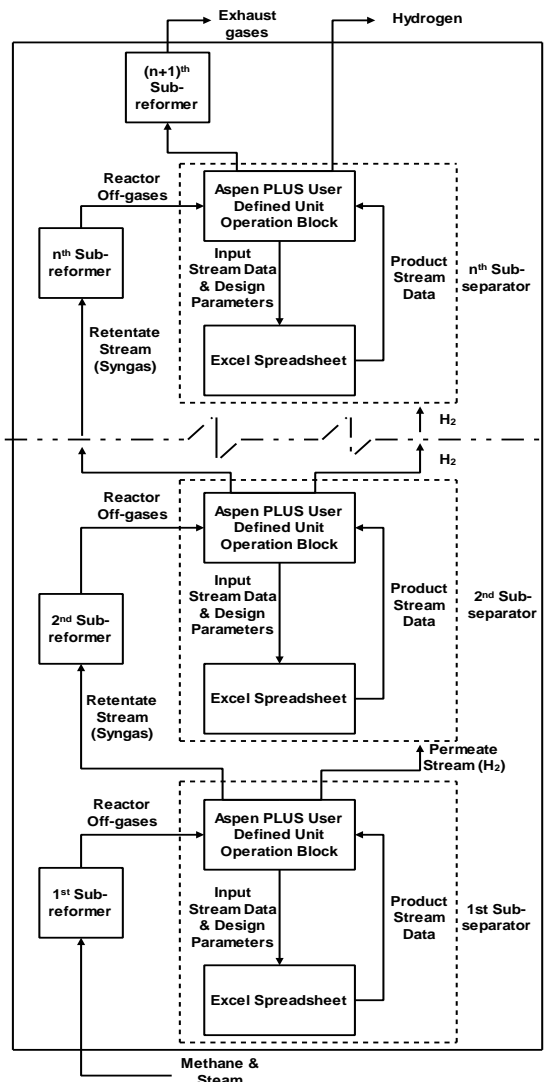


Fig. 5: A schematic diagram of sequential modular simulation of overall FBMR process.

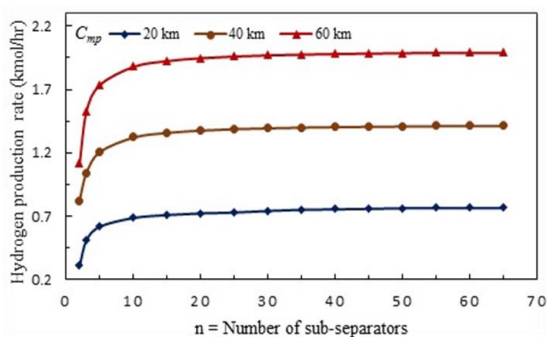


Fig. 6: Influence of number of sub-separators on hydrogen production rate.

($F_{CH_4} = 1$ kmol/h, $T = 600$ °C, $P = 2$ MPa, Steam feed rate = 3 kmol/h, $\eta = 1$, $P_{MH_2} = 0.1$ MPa)

Table-2 shows that the model predicts the experimental data within an acceptable accuracy and there is a minor deviation between the results predicted by the model and experimental results. The predictions of the current model were also compared with the results predicted by Ye (2009) model [21]. It can be seen that the predictions of both models are also in good agreement.

Table-2: Comparison of model predictions with experimental data of Adris (1994) and predicted results of Ye (2009) model.

($F_{CH_4} = 74.2$ mol/h, Steam feed rate = 178.08 mol/h, $C_{mp} = 0.4$ km, $P = 0.98$ MPa, Sweep gas flow rate = 80 mol/h, $\eta = 0.39$).

Bed Temperature (K)	720	767	815	867	913	
Experimental						
Methane conversion	12	18	26.4	36.6	47.9	
X_{CH_4} (%)	11.3	16.4	23	32	41.5	
Experimental						
Hydrogen production rate Q_{H_2} (mol/h)	1.7	2.5	3.5	4.81	6.23	
Experimental						
Product gas composition (Vol %, dry basis)						
Experimental						
CH ₄	Predicted by Ye model	61.7	49.6	37.6	27.3	19.5
	Predicted by current model	62.2	51.9	41.8	31.8	23.8
	Predicted by current model	62.7	52.3	42.3	32.1	24
Experimental						
CO	Predicted by Ye model	0.1	0.4	1.2	3.2	5.6
	Predicted by current model	0.2	0.5	1.2	2.7	4.8
	Predicted by current model	0.3	0.5	1.24	2.6	4.7
Experimental						
H ₂	Predicted by Ye model	28.7	38.5	48.2	56	61.6
	Predicted by current model	29.8	37.8	45.7	53.3	59.2
	Predicted by current model	29.4	37.6	45.9	55.3	59.5
Experimental						
CO ₂	Predicted by Ye model	9.5	11.5	13	13.5	13.3
	Predicted by current model	7.7	9.6	11.2	12.1	12.1
	Predicted by current model	7.6	9.5	10.8	11.7	11.7

Results and Discussions

Influence of Operating Parameters on Reactor Performance

The major operating parameters like reactor temperature, pressure, permeate side hydrogen partial pressure and steam feed rate, and design parameters like membrane area are investigated for both the reactors and compared with each other. Due to safety and economic limitation, these parameters cannot be studied beyond the range of parameter that can be studied experimentally. The parameters are studied well above the experimental range to test the reactors' performance. The influence of these

parameters on hydrogen yield (molar pure H_2 production rate/molar CH_4 feed rate) and methane conversion for FBMR based on palladium and nickel membranes were predicted and compared.

Influence of Reactor Temperature

The influence of reactor temperature on methane conversion for different membrane permeation capacities is shown in Fig 7. It can be seen that for both palladium-based and nickel-based FBMR methane conversion increases with temperature. The 0 C_{mp} line shows FBMR without hydrogen separation and simply represents a conventional reformer. The conventional reformers are operated between 450-850 °C while the operating temperature range of membrane reformers depend upon the stability of membrane which is used inside the reactor [16]. For palladium-based FBMR, the results are plotted up to 650 °C. It cannot be operated beyond 650 °C due to the interaction of the palladium membrane with its support [17]. The results are plotted up to 850 °C for the nickel-based FBMR due to its stability at much higher temperature (1000 °C) as compared to the palladium-based membranes [14]. In Fig 7, it can be seen that both nickel based and palladium based FBMR achieve higher methane conversion at a lower temperature than conventional reformer due to the removal of hydrogen from reaction products. The Fig also shows that nickel-based FBMR has lower methane conversion than palladium-based FBMR. According to equation (4), at a constant temperature, hydrogen permeation rate decreases exponentially with the increase of activation energy (energy required to adsorb hydrogen atom on membrane surface). The activation energy required for nickel membrane ($-51070 \text{ J mol}^{-1}$) is higher than palladium membrane (-9180 J mol^{-1}). As a result, nickel membrane removes less amount of hydrogen from the reaction products and has lower methane conversion than the palladium-based membrane reactor. The influence of temperature on methane conversion at higher permeation capacities (80 C_{mp}) is significant for both membrane reactors.

Fig. 8 shows the influence of reactor temperature on hydrogen yield. It can be seen that the hydrogen yield increases with increasing reactor temperature. The influence of reactor temperature on hydrogen yield is much more significant at higher membrane permeation capacities. The nickel-based FBMR has a lower hydrogen yield as compared to the palladium-based FBMR. The reason is the higher activation energy of nickel-based membranes which is required for the diffusion of hydrogen through the membrane. To obtain hydrogen yield comparable to

the one obtained through the palladium-based FBMR, the nickel-based FBMR should be operated at higher temperature or with larger surface area.

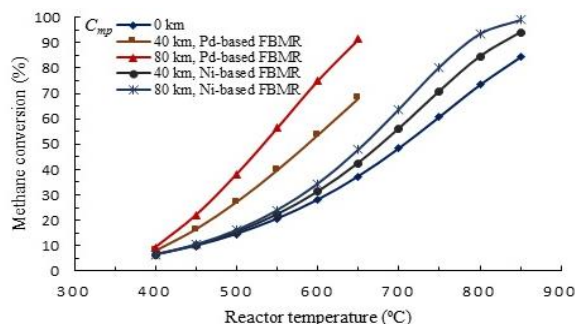


Fig. 7: Influence of reactor temperature on methane conversion.

($F_{CH_4} = 1 \text{ kmol/h}$, $P = 2 \text{ MPa}$, Steam feed rate = 3 kmol/h , $\eta = 1$, $P_{MH_2} = 0.1 \text{ MPa}$)

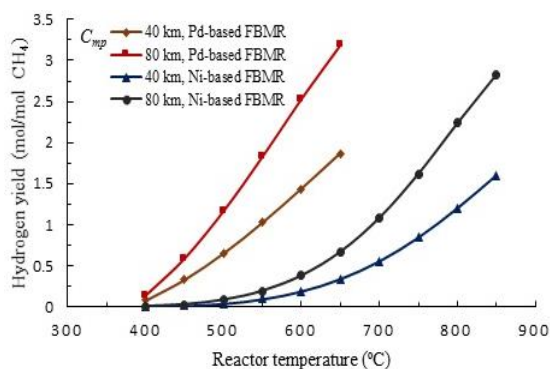


Fig. 8: Influence of reactor temperature on hydrogen yield.

($F_{CH_4} = 1 \text{ kmol/h}$, $P = 2 \text{ MPa}$, Steam feed rate = 3 kmol/h , $\eta = 1$, $P_{MH_2} = 0.1 \text{ MPa}$)

Influence of Pressure

The thermodynamic equilibrium of methane reforming reactions follows Le Chatelier's principle, so that low-pressure benefit reaction 1 and 3, whereas, reaction 2 is independent of pressure. The membrane installed in FBMR reduces the adverse effect of high pressure by removing hydrogen from reaction products. The high pressure in FBMR also creates a high driving force for hydrogen permeation. The influence of reactor pressure on methane conversion is shown in Fig 9. At 0 C_{mp} , with increasing reactor pressure conversion decreases, indicating the behavior of conventional reformer according to the Le Chatelier's Principle. For FBMR

based on palladium membrane, it can be seen that for lower permeation capacity ($40 C_{mp}$), methane conversion decreases up to 1 MPa due to the adverse effect of pressure but as the pressure is increased beyond 1 MPa the driving force for hydrogen permeation dominates the adverse effect of pressure and methane conversion increases. At higher permeation capacities ($80 C_{mp}$), a linear increase occurs in methane conversion with increasing pressure. For FBMR based on nickel membrane, the methane conversion decreases up to 3.5 MPa due to the adverse effect of pressure. Further increase in pressure produces no increase in methane conversion and the conversion remains almost constant. The reason is the lower permeation rate of hydrogen through nickel membranes as compared to palladium membranes. The hydrogen permeation rate (removal of product moles) through nickel membranes are to an extent that can only balance the adverse effect of high pressure but cannot dominate it. This trend of methane conversion with pressure for nickel-based FBMR is more prominent for higher permeation capacity ($80 C_{mp}$). The influence of reactor pressure on hydrogen yield is shown in Fig 10. It can be seen that hydrogen yield increases with increasing reactor pressure for all permeation capacities. Hydrogen production rate is much higher for palladium-based FBMR as compared to nickel-based FBMR at the same operating temperature and pressure.

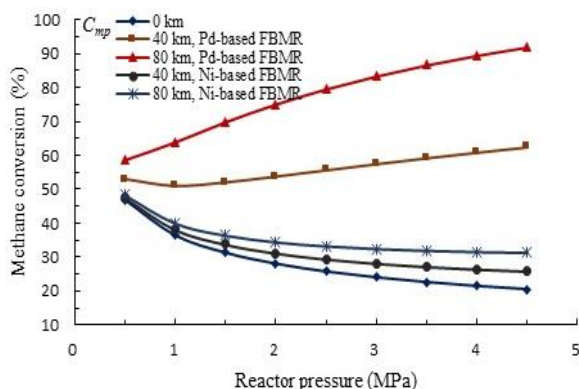


Fig. 9: Influence of reactor pressure on methane conversion.

($F_{CH_4} = 1$ kmol/h, $T = 600$ °C, Steam feed rate = 3 kmol/h, $\eta = 1$, $P_{MH_2} = 0.1$ MPa.)

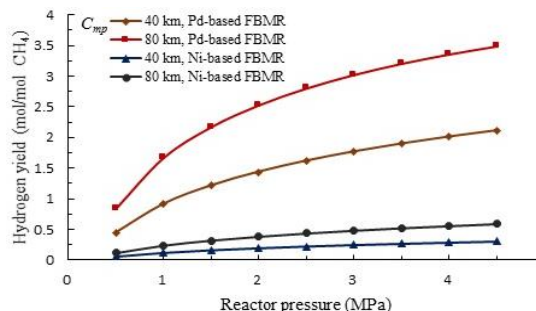


Fig. 10: Influence of reactor pressure on hydrogen yield.

($F_{CH_4} = 1$ kmol/h, $T = 600$ °C, Steam feed rate = 3 kmol/h, $\eta = 1$, $P_{MH_2} = 0.1$ MPa.)

Influence of Permeate Side Hydrogen Partial Pressure

A sweep gas is used or vacuum is employed to reduce permeate side hydrogen partial pressure. It can be seen in Fig 11 that decreasing permeate side hydrogen partial pressure increases methane conversion. Increase in methane conversion with decreasing hydrogen partial pressure is more likely occurring for palladium-based FBMR while for nickel-based FBMR the increase in methane conversion is very small due to much lower hydrogen permeability through nickel membranes. At higher permeation capacities ($80 C_{mp}$), the influence on methane conversion is more significant. A similar trend is observed for hydrogen yield in Fig 12. Hydrogen yield increases with decreasing permeate side hydrogen partial pressure for both reactors and the influence on hydrogen yield is more significant for higher permeation capacities.

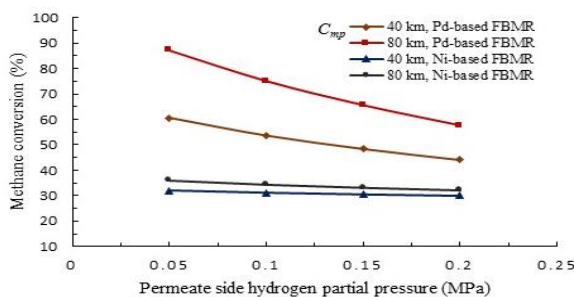


Fig. 11: Influence of permeate side hydrogen partial pressure on methane conversion.

($F_{CH_4} = 1$ kmol/h, $T = 600$ °C, $S/C = 3$, $\eta = 1$, $P = 2$ MPa.)

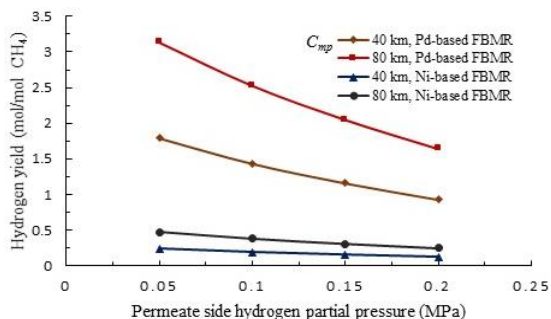


Fig. 12: Influence of permeate side hydrogen partial pressure on hydrogen yield.

($F_{CH_4} = 1$ kmol/h, $T = 600$ °C, $S/C = 3$, $\eta = 1$, $P = 2$ MPa.)

Influence of Steam Feed Rate

High steam feed rate could increase methane conversion according to Le Chatelier's principle. The influence of steam feed rate on methane conversion is shown in Fig 13. It can be seen that methane conversion increases with increasing steam feed rate for both reactors. However, hydrogen yield nearly remains constant with increasing steam feed rate and does not seem to be significantly influenced by steam feed rate as illustrated in Fig 14. Methane conversion increases with increasing steam feed rate but, high steam feed rate reduces hydrogen partial pressure in the reactor, which reduces the driving force for hydrogen permeation through membrane tubes. These two counteracting effects (high methane conversion and reduced hydrogen partial pressure) balance each other and as a result, there is a little influence of steam feed rate on hydrogen yield.

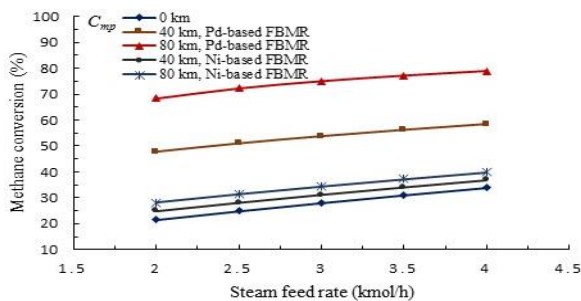


Fig. 13: Influence of steam feed rate on methane conversion.

($F_{CH_4} = 1$ kmol/h, $P_{MH_2} = 0.1$ MPa, $T = 600$ °C, $\eta = 1$, $P = 2$ MPa.)

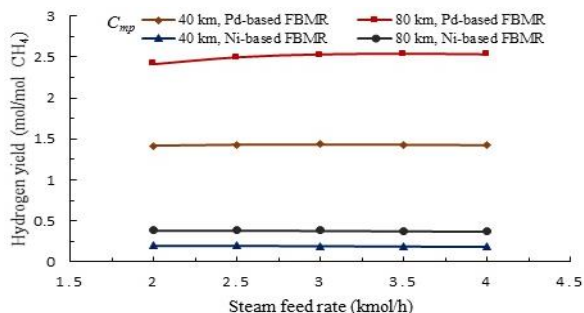


Fig. 14: Influence of steam feed rate on hydrogen yield.

($F_{CH_4} = 1$ kmol/h, $P_{MH_2} = 0.1$ MPa, $T = 600$ °C, $\eta = 1$, $P = 2$ MPa.)

Comparison between Nickel-based and Palladium-based FBMR

Fig 15 shows the comparison between nickel-based and palladium-based FBMR in terms of methane conversion. The two reactors having the same membrane area installed are operated at the same operating conditions. It can be seen that palladium-based FBMR achieves 68.2 % methane conversion at 650 °C while nickel-based FBMR achieves this conversion at a higher temperature (748 °C). Similarly, it can be seen in Fig 16 that nickel-based FBMR produces 1.86 mol/mol CH_4 at much higher temperature than palladium-based FBMR. The operating cost of the process is reduced in case of both the membrane reactors as compared to the conventional reformer but the nickel-based FBMR has still higher operating cost than palladium-based FBMR. To achieve 68.2 % methane conversion with hydrogen yield of 1.86 mol/mol CH_4 , nickel-based FBMR should be operated with higher membrane area.

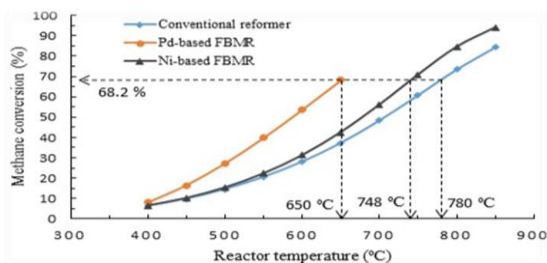


Fig. 15: Influence of reactor temperature on methane conversion.

($F_{CH_4} = 1$ kmol/h, $P = 2$ MPa, $A_m = 8$ m², $S/C = 3$, $\eta = 1$, $P_{MH_2} = 0.1$ MPa)

Required Membrane Area and Cost Analysis

The main parameter on which cost of membrane tubes depends is the price of raw material. Having a membrane surface area and membrane thickness, the weight and cost of raw material can then be estimated. Fig 17 shows the influence of membrane area on methane conversion in nickel-based FMBR. It can be seen that methane conversion increases linearly with increasing membrane area. The graph shows that about 49 m² membrane area should be installed within nickel-based FMBR to achieve 68.2 % methane conversion with hydrogen yield of 1.87 mol/mol CH₄ which are achieved by palladium-based FMBR with only 8 m² membrane area. The nickel-based membrane, the required area is about 6.1 times larger than the palladium membrane area required. On the other hand, the market price of palladium is 2300 \$/100g which is 2300 times more expensive than nickel (nickel price, 1.1 \$/100g) [18, 19]

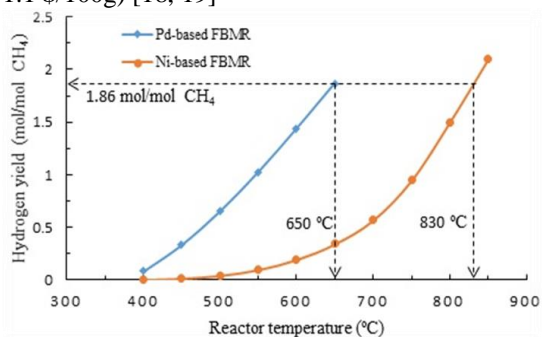


Fig. 16: Influence of reactor temperature on methane conversion.

($F_{CH_4} = 1$ kmol/h, $P = 2$ MPa, $A_m = 8$ m², $S/C = 3$, $\eta = 1$, $P_{MH_2} = 0.1$ MPa)

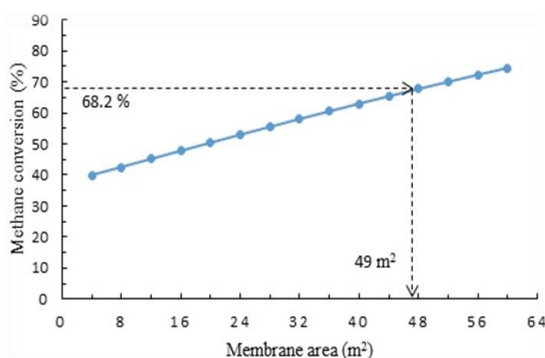


Fig. 17: Influence of nickel membrane area on conversion.

($F_{CH_4} = 1$ kmol/h, $P = 2$ MPa, $T = 650$ °C, $S/C = 3$, $\eta = 1$, $P_{MH_2} = 0.1$ MPa.)

Conclusion

A nickel-based fluidized bed membrane reactor model for steam methane reforming is developed and simulated within Aspen PLUS®. The simulated results of the model are compared with the palladium-based fluidized bed membrane reactor for methane conversion and hydrogen yield. The results indicated that at about 748 °C, nickel-based FMBR achieved 68.2 % methane conversion which is achieved by palladium-based FMBR at 650 °C. It was found that about 6.1 times larger surface area is required for the nickel-based FMBR than the palladium-based FMBR to achieve the same methane conversion at the same operating conditions. However, the substantially lower price of nickel, stability at higher operating temperature and its resistance towards sulfur, steam and carbon monoxide makes it a suitable alternative to be used in steam reforming membrane reactors.

Nomenclature

FMBR	Fluidized bed membrane reactor	Q_{H_2}	Hydrogen permeation rate
SC	Steam to carbon ratio	η	Permeation effectiveness factor
N	Number of sub-separators used	k	Pre-exponential factor
F_{CH_4}	Methane feed rate	C_{mp}	Membrane permeation capacity
X_{CH_4}	Methane conversion	P_{RH_2}	Reactor side hydrogen partial pressure
T	Reactor temperature	P_{MH_2}	Membrane side hydrogen partial pressure
P	Reactor pressure	E_a	Activation energy
R	Ideal gas constant		

References

1. A. Adris, C. Lim, and J. Grace, The fluidized-bed membrane reactor for steam methane reforming: model verification and parametric study, *Chem. Eng. Sci.*, **52**, 1609 (1997).
2. C. S. Patil, M. van Sint Annaland, and J. A. Kuipers, Design of a novel autothermal membrane-assisted fluidized-bed reactor for the production of ultrapure hydrogen from methane, *Ind. Eng. Chem. Res.*, **44**, 9502 (2005).
3. A. Santucci, F. Borgognoni, M. Vadrucchi, and S. Tosti, Testing of dense Pd–Ag tubes: Effect of pressure and membrane thickness on the hydrogen permeability, *J Memb Sci*, **444**, 378 (2013).
4. K. Babita, S. Sridhar, and K. Raghavan, Membrane reactors for fuel cell quality hydrogen through WGSR—Review of their status, challenges and opportunities, *Int. J. Hydrog. Energy*, **36**, 6671-6688 (2011).

5. J. Shu, B. P. Grandjean, and S. Kaliaguine, Methane steam reforming in asymmetric Pd-and Pd-Ag/porous SS membrane reactors, *Appl. Catal., A*, **119**, 305 (1994).
6. M. Abashar, Coupling of steam and dry reforming of methane in catalytic fluidized bed membrane reactors, *Int. J. Hydrog. Energy*, **29**, 799 (2004).
7. M. Dogan, D. Posarac, J. Grace, A.-E. M. Adris, and C. J. Lim, Modeling of autothermal steam methane reforming in a fluidized bed membrane reactor, *Int J Chem React Eng*, **1** (2003).
8. S. Roy, *Fluidized bed steam methane reforming with high-flux membranes and oxygen input* (University of Calgary, 1998).
9. J. R. Grace, X. Li, and C. J. Lim, Equilibrium modelling of catalytic steam reforming of methane in membrane reactors with oxygen addition, *Catal Today*, **64**, 141 (2001).
10. Z. Chen and S. S. Elnashaie, Steady-state modeling and bifurcation behavior of circulating fluidized bed membrane reformer–regenerator for the production of hydrogen for fuel cells from heptane, *Chem. Eng. Sci.*, **59**, 3965 (2004).
11. S. Yun and S. T. Oyama, "Correlations in palladium membranes for hydrogen separation: a review," *J Memb Sci*, **375**, 28 (2011).
12. A. Adris, C. J. Lim, and J. Grace, The fluidized bed membrane reactor system: a pilot scale experimental study, *Chem. Eng. Sci.*, **49**, 5833 (1994).
13. A. Basile and F. Gallucci, *Membranes for membrane reactors: preparation, optimization and selection* (John Wiley & Sons, 2010).
14. M. Wang, J. Song, X. Wu, X. Tan, B. Meng, and S. Liu, Metallic nickel hollow fiber membranes for hydrogen separation at high temperatures, *J Memb Sci*, **509**, 156 (2016).
15. A. Unemoto, A. Kaimai, K. Sato, T. Otake, K. Yashiro, J. Mizusaki, T. Kawada, T. Tsuneki, Y. Shirasaki, and I. Yasuda, Surface reaction of hydrogen on a palladium alloy membrane under co-existence of H₂O, CO, CO₂ or CH₄, *Int. J. Hydrog. Energy*, **32**, 4023-4029 (2007).
16. A. Mahecha-Botero, T. Boyd, A. Gulamhusein, N. Comyn, C. J. Lim, J. R. Grace, Y. Shirasaki, and I. Yasuda, Pure hydrogen generation in a fluidized-bed membrane reactor: experimental findings, *Chem. Eng. Sci.*, **63**, 2752-2762 (2008).
17. N. D. Deveau, Y. H. Ma, and R. Datta, Beyond Sieverts' law: a comprehensive microkinetic model of hydrogen permeation in dense metal membranes, *J Memb Sci*, **437**, 298-311 (2013).
18. Palladium Price Today | Price of Palladium Per Ounce | 24 Hour Spot Chart | KITCO. [Online]. Available: <http://www.kitco.com/charts/livepalladium.html>. [Accessed: 28-Jan-2017]
19. Nickel Prices and Nickel Price Charts - Investment Mine. [Online]. Available: <http://www.infomine.com/investment/metal-prices/nickel/>. [Accessed: 28-Jan-2017]
20. Sarvar-Amini, A., Sotudeh-Gharehagh, R., Bashiri, H., Mostoufi, N., Haghtalab, A., Sequential simulation of a fluidized bed membrane reactor for the steam methane reforming using Aspen Plus, *Energy Fuels*, **21**, 3593 (2007).
21. Ye, G., Xie, D., Qiao, W., Grace, J.R., Lim, C.J., Modeling of fluidized bed membrane reactors for hydrogen production from steam methane reforming with Aspen Plus, *Int. J. Hydrog. Energy*, **34**, 4755 (2009).